Available online at www.sciencedirect.com
SCIENCE DIRECT®
Polymer 44 (2003) 5877–5884
polymer
www.elsevier.com/locate/polymer

Structure and deformation mechanisms in UHMWPE-fibres

L. Berger[1], H.H. Kausch*, C.J.G. Plummer

Institut des Matériaux, Ecole Polytechnique Fédérale de Lausanne, CH-1015 Lausanne, Switzerland

Received 27 January 2003; accepted 24 March 2003

Dedicated to Prof. Ian M. Ward on the occasion of his 75th birthday

Abstract

Raman microscopy is applied to a gel-spun UHMWPE-fibre (Dyneema SK60) to determine the distribution of axial molecular stresses and their change with time (in creep and during stress relaxation). A more detailed method is proposed to quantify the observed characteristic changes in local stress distribution. The increase in highly overstressed bonds (5–8 GPa) is ascribed to the straining of tie-molecules during creep. Their pull-out, crystal plasticity and grain-boundary slip determine stress relaxation. A refined structural model of the UHMWPE-fibre is proposed, which is used to discuss the still existing difference between theoretical and practical strength of such fibres.

Keywords: UHMWPE-fibre; Raman microscopy; Tie-chain pull-out

1. Introduction

The characteristic properties of macromolecules—great length, large anisotropy and high segmental flexibility—give rise to a complex structural organisation and to unique properties. The weak lateral coherence of strong chain segments offers an enormous potential for processing at comparatively low temperatures and it is an essential condition for rubber elastic and viscoelastic behaviour [1,2]. The same characteristics are also responsible for the strong dependence of macroscopic performance on molecular orientation; thus Young's modulus and tensile strength of amorphous as well as of semi-crystalline solids increase by orders of magnitude as a function of the degree of orientation [3,4]. Segmental strength, crystallisability and flexibility are also a prerequisite for the formation of high performance fibres [5–7]. *Natural fibres* are based on this concept; they exist and have been used *forever*. *Man-made fibres* are known for about 120 years; properties and produced quantity have increased enormously from Rayon (regenerated cellulose, 1884) over nylon (1938), PAN-based carbon fibres (1962), Kevlar™ or other aromatic fibres (1965) to present-day ultra-high strength fibres (such as single crystal polydiacetylene or PBZO fibres) [6,8,9].

All the fibre species cited above had been created by novel methods of synthesis; they owe their increased strength and/or stiffness to specific features of polymer backbone configuration (such as conjugated double bonds or aromatic rings). Following a different route, Capaccio and Ward obtained a notable improvement of mechanical properties of polyethylene by achieving high draw ratios through the multiple stage hydrostatic melt extrusion process [10]. At about the same time ultra highly oriented high molecular weight polyethylene—UHMWPE—fibres were obtained by two other processing techniques: by drawing from solution [11] and by gel-spinning [12]. Because of their high strength to weight ratio UHMWPE fibres are excellent materials for weight-sensitive applications like towing lines, helmet reinforcement or sails. And the chemical identity of UHMWPE with HDPE makes them ideal candidates for self-reinforced PE–PE composites [13,14]. The major disadvantage of PE fibres is their sensitivity to creep due to the small cohesive energy density of PE and the presence of structural irregularities.

In this investigation Raman microscopy is used to determine the distribution of axial molecular stresses and their change with time (in creep and during stress relaxation). It is then attempted to associate the observed characteristic changes in local stress distribution to elements of the fibre microstructure. This way the nature of the deformation mechanisms and their effect on macroscopic strength will become accessible.

* Corresponding author. E-mail: hans-henning-kausch@epfl.ch.
[1] Present address: Alcan Airex AG, CH-5643 Sins, Switzerland.

0032-3861/03/$ - see front matter © 2003 Published by Elsevier Ltd.
doi:10.1016/S0032-3861(03)00536-6

2. Materials and microstructure

The material used throughout this study was a gel-spun UHMWPE-fibre (Dyneema SK60, produced by DSM High Performance Fibres, Holland) having a molecular weight of $2-2.5 \times 10^6$ Da. The fibre consists of 780 single filaments having a coarseness of 800 den (Fig. 1). The cross-section of a filaments is not circular, but bean- or kidney-shaped (with an average area of 115 μm^2). Such a filament shows a substructure typically 150 *macro*fibrils.

Concerning the microstructure of a macrofibril essentially two models can be found in the literature. In the first a *macro*fibril is believed to consist of highly extended chains forming crystalline *micro*fibrils having a diameter of 15 to 20 nm (*microfibrillar model*). In the *continuous crystalline model*, on the other hand, it is assumed that the macrofibrils consist of a more or less continuous crystalline phase with dispersed and rare defects [12]. The very high degree of chain orientation is well demonstrated by the high-resolution TEM micrograph of a gel spun hot drawn film of UHMWPE (Fig. 2).

UHMWPE fibres are highly ordered, but are not *mono*-crystalline. For the SK60 fibre Berger [15] has determined from density measurements that there is a fraction about 25% of non-crystalline material. This fraction comprises of highly extended but non-crystalline segments (having a density of 0.90 g/ml), the rare entanglements (about 2.5 per molecule) and folds. The value of 25% roughly agrees with the degree of crystallinity determined from the melting enthalpy (71%). The crystalline phases were identified as orthorhombic (85%) and monoclinic (15%). From NMR experiments it had been concluded that the amorphous phase is accounting for less than 5% of the material [16]. The absence of an amorphous X-ray halo indicates an even

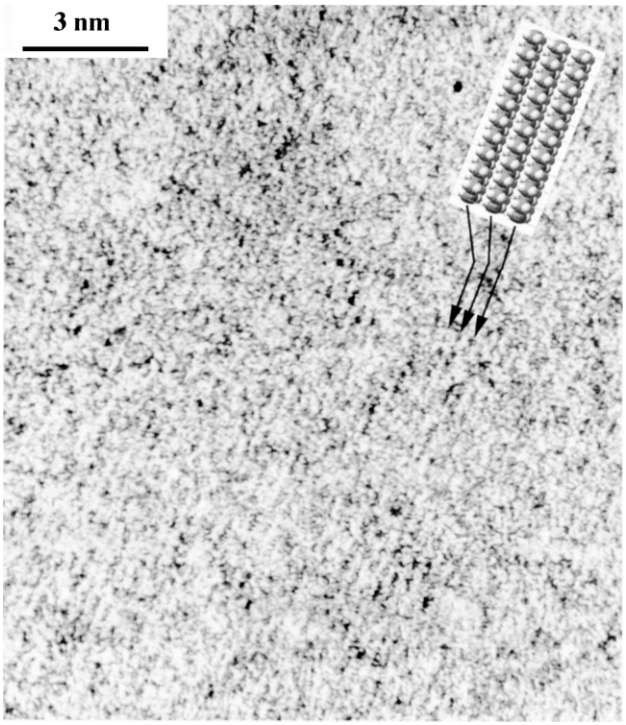

Fig. 2. High-resolution TEM micrograph of a gel-spun hot drawn film of UHMWPE.

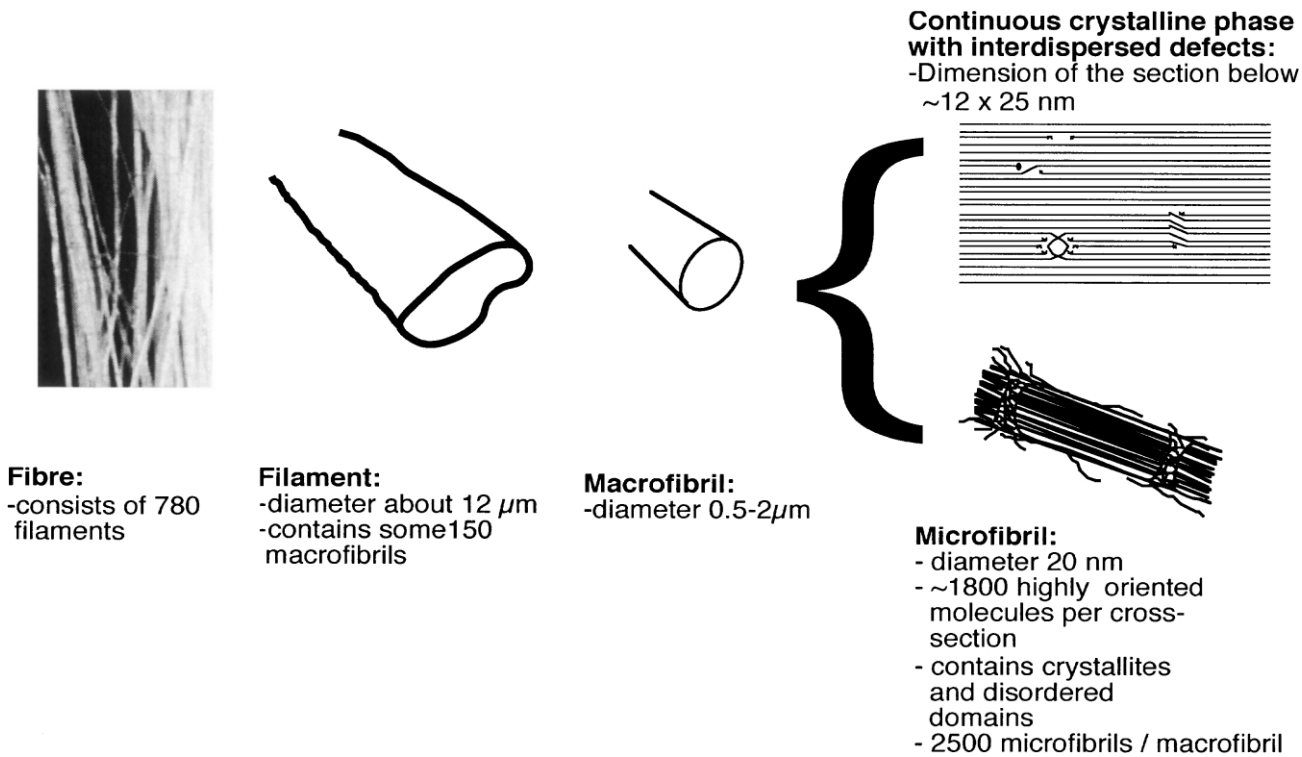

Fig. 1. Substructure of a gel-spun Dyneema SK60 fibre.

smaller fraction [15,17]. The above data show that the amorphous component cannot be expected to form a coherent phase, more likely it comprises all the less ordered segments, tie molecules, conformational irregularities (out of register, twists, rare entanglements) and *defects* in the crystalline phases and at the boundaries and interfaces of microfibrils. Evidently the morphology of highly oriented fibres depends on the starting material (chain length and linearity, degree of entanglement, crystalline morphology) [7,18] and on the applied processing technique (solid state or melt extrusion, gel spinning, hot drawing) [7,10–12,18,19].

The difference between the two structural models lies in the intensity of (lateral) stress transfer between microfibrils. Microfibrils behave as structural entities only if the lateral interaction is smaller than the intra-microfibrillar cohesion. The crystalline bridge model of Ward combines both aspects; it allows for strong lateral interaction across a microfibrillar interface through crystalline regions, and for a much weaker interaction with the non-crystalline regions [20]. With small individual variations this concept is widely used [21–25] and it will also be employed in this work (Fig. 3). A review of the different structural models of highly drawn polymers has been given Porter and Wang [7].

The regions A and B represent fully chain-extended crystalline regions; for the elastic modulus values of between 255 to 315 GPa are indicated in the literature [15,24,26] with a preferred value of 290 GPa [24]. Region C represents the fraction of slightly disordered chain segments, which are non-crystalline (although most of them are well extended). As indicated above, in SK 60 fibres the fraction of non-crystalline material amounts to about 25%. It is reasonable to assume that this phase contains intra-microfibrillar tie-molecules of various degrees of tautness. The tie-molecules are capable to transmit important axial stresses (the pull-out stress of a tie-molecule from a defect-free orthorhombic crystal amounts to 7.5 GPa [27]).

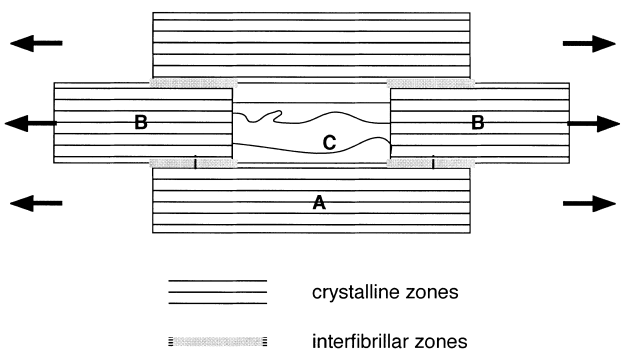

Fig. 3. Two-dimensional mechanical model of a macrofibril of UHMWPE showing the essential structural elements: crystalline regions, inter-microfibrillar zones, and non-crystalline regions containing more or less taut tie-molecules (the possible slight misalignments, distortions, and variations in width of microfibrils are not shown; see text for the size of the crystalline regions).

Stresses between the crystalline blocks B are also transferred by shear through the interfaces i and region A. Concerning the size of the crystals in UHMWPE-fibres, the *lateral dimensions* were found to decrease with draw ratio to a value of about 13 to 15 nm [26,28]; the crystalline *length in chain direction*, however, seems to depend strongly on the fibre type. Using WAXD, Nakamae found in Dyneema-fibres a length of 71 nm [26], Grubb et al. reported values of respectively, 5–13 nm for Spectra 900 fibres, and 15–43 nm for Spectra 1000-fibres [28].

In the following we determine the distribution of molecular stresses for the three standard loading modes (creep, relaxation, loading at constant strain rate).

3. Experimental procedure

3.1. Mechanical testing

Single filaments and fibre bundles were tested using a Zwick 1484 tensile test machine and an in-house-built mini-tensile test machine, as described elsewhere [15]. The deformation was measured by optical extensometry using a video camera connected to an image processing computer. By this technique the real deformation of the sample is measured and slippage in the clamping system does not interfere with the evaluation.

3.2. Raman spectroscopy

The position and form of Raman bands assigned to C–C stretching vibrations change with the application of tensile stress to the chain backbone. This stress sensitivity allows investigation of the molecular stress distribution by Raman spectroscopy [15,24,29,30]. In polyethylene, the bands at 1060 and 1130 cm^{-1} exhibit the greatest peak shift upon mechanical deformation. In our investigations we have used the symmetric stretching band at 1130 cm^{-1}, for which we have determined a peak shift value of -5.73 cm^{-1}/GPa [15]. Using this shift factor the wave number axis can be converted into a stress axis (Fig. 4(a)). The subsequent transformation into stress *intensities* is generally achieved by fitting the deformed Raman band by a number (two or three) Lorentzian peaks [30]. In our approach we have used about 20 Lorentzian peaks having a width corresponding to the width of the peak of an undeformed sample, and which were separated on the converted wavenumber axis by 0.5 Gpa from each other (Fig. 4).

All measurements were undertaken on single SK60 filaments at room temperature on a DILOR XY800 Raman spectrometer as described elsewhere [15]. To deform the samples the above mentioned mini tensile test machine was used. The deformation was measured with optical extensometry. Since a liquid nitrogen cooled CCD camera was used as a detector, the integration time needed to obtain a good spectrum was as short as 20 s.

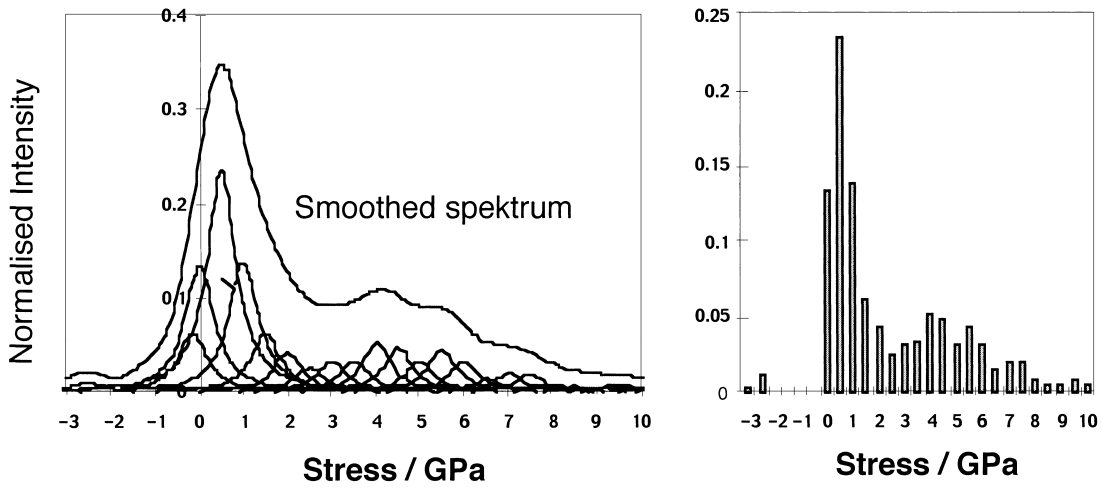

Fig. 4. Transformation of a converted, deformed Raman band (of a fibre loaded to 2 GPa) into a stress histogram by curve fitting with Lorentzian peaks [15].

4. Results and discussion

4.1. Creep

The creep of single filaments of an SK60-fibre has been studied in the stress range 0.65–2 GPa for a period of 30 h (Fig. 5).

The instantaneous elastic modulus E of the SK60 filaments during creep test was measured by partially unloading and reloading the sample during the test (Fig. 5). A notable increase (from some 60 to more than 120 GPa) is observed during the first 30 s under load (Fig. 6). Afterwards the instantaneous modulus slowly decreases. This behaviour can be explained by two competing processes: the *elimination of strain inhomogeneities* and anelastic deformation (on the microscopic and/or molecular level) and by uncorrelated *slip* (of parts of a microfibril or of highly loaded chains). The straightening-out of intra- and inter-microfibrillar tie-molecules leads to an increase of overall modulus of the fibre. Most of this deformation turns out to be reversible. In later stages pull-out of tie-molecules and correlated intra-crystalline slip will have the opposite effect, a slow but systematic decrease of the modulus.

This interpretation is also confirmed by a Sherby–Dorn plot of the creep curves. Two distinct regions can clearly be seen: a sharp decrease of the creep rate with increasing strain generally assigned to reversible viscoelastic creep deformation [15,20,21] and a plateau region of irreversible plastic flow generally assigned to intra-crystalline slip (Fig. 7). The creep rate increases with stress in a non-linear manner, for gel-spun fibres it is smaller than that of melt-spun fibres [31,32]. Using a high resolution Doppler creep rate meter Mjasnikova et al. have shown that the apparently stationary creep rate in some UHMWPE fibres is in reality a succession of inter-microfibrillar deformation jumps at intervals of 10 and 50–70 μm respectively; the creep rates within a deformation jump can be an order of magnitude higher than the average rate [32].

The effect of transient deformation mechanisms is also seen in cyclic loading experiments, where the elastic modulus of the fibre increases from the first to the second cycle, afterwards it decreases. Since the most important *strain inhomogeneities* are reduced in the first cycle the dispersed energy (hysteresis loop) decreases subsequently [15,22].

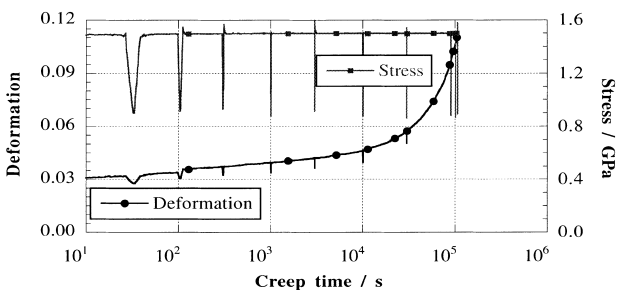

Fig. 5. Creep curve of a single filament of SK60 at 1.5 GPa. The instantaneous modulus had been determined by rapidly discharging to 1 GPa and subsequent reloading.

4.2. Raman spectroscopy

In the following we shall discuss three modes of loading, creep, stress relaxation and loading at constant strain rate. The unstressed fibre shows a stress histogram with a sharp maximum at zero stress. The spectrum of a fibre recorded

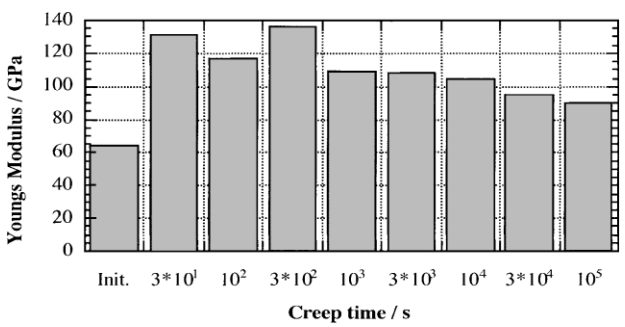

Fig. 6. Development of the instantaneous modulus during creep.

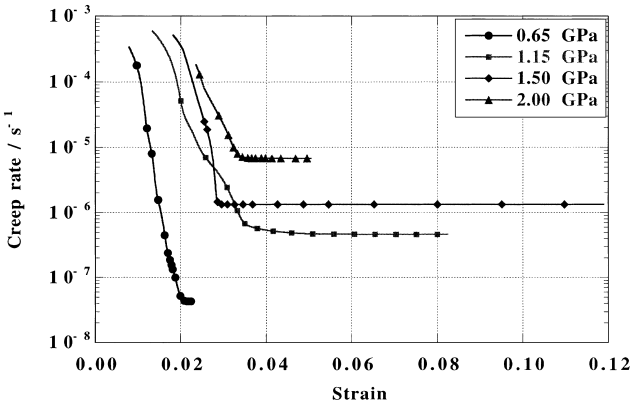

Fig. 7. Sherby–Dorn plot of the creep of SK60 filaments.

immediately after application of a stress of 1.5 GPa has typically the shape shown in Fig. 4, which resembles a bimodal distribution. Most segments are loaded to between 0 and 1 GPa, 25% of the population to between 1.5 and 4 GPa and 2.5% to stresses between 5 and 10 GPa. During creep this distribution changes, the bimodal character being reinforced. Fig. 8 shows three difference spectra from a creep test at 1.5 GPa (the spectrum taken immediately after loading has been subtracted from the spectra taken after creep time of about 36 min, 2 h and 18 h). The number of weakly (0–1 GPa) and highly loaded segments (4.5–10) increases at the expense of segments loaded with moderate overstress (1.5–4 GPa).

This observation can be explained on the basis of the structural model in Fig. 3. The increase in highly stressed bonds from 2.5 to 6% after 2 h is assigned to an increase in the number of *taut* intra-microfibrillar tie molecules during elongation of the fibre (due to the separation of phases B) or of taut inter-microfibrillar ties (following inter-microfibrillar slip). The decrease of moderately overstressed bonds in our fibres is apparently due to the limitation of strain in region A, either due to slip at the interfaces i or to crystal plasticity. This mechanism seems to be at the origin of the generally observed bimodal stress distribution. There is a first population of crystalline regions, which we believe to

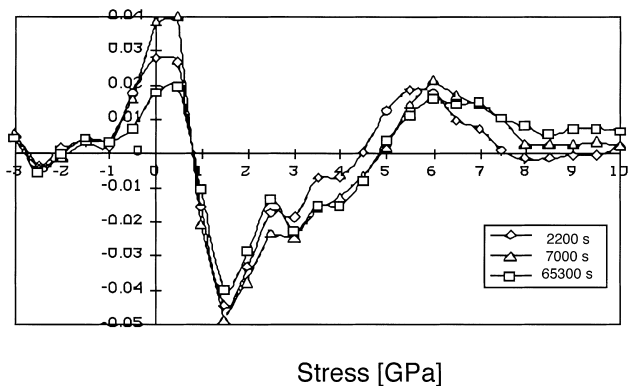

Fig. 8. Raman difference spectra from a creep test at 1.5 GPa indicating the changes in stress population occurring during creep periods of 2200, 7000, and 65,300 s, respectively.

be intimately connected with tie-molecules, which deform to strains of up to 2% with associated stresses of 4–6 GPa [15,24,29,33]. According to the calculations of Kausch and Langbein [4,27] there is an upper limit of 7.5 GPa for the axial stress that can be imposed on a tie-molecule through a perfect orthorhombic crystal. At this stress the chain begins to be pulled out of the crystal creating a defect, which runs all the way through the crystal until it hits an obstacle such as a fold or an entanglement. When this occurs stresses can even be built up to higher values than 7.5 GPa. This would explain the fraction of highly loaded segments detected in the above Raman spectra.

Besides the small fraction of highly loaded crystalline regions there is a second and larger population of crystals, which show a distinct and smaller upper strain limit. As a function of macroscopic stress their *c*-axis will be stretched homogeneously up to a temperature-dependant critical strain of 0.4 to 0.6% [15,24,29,33]. In our case, the critical strain amounts to 0.4 and 0.43% [15,33]. This corresponds to a stress of 1.2 GPa. The fact that stresses are preferably relieved from segments stressed to beyond 1 GPa and that strains of 0.4% are maintained in a stress relaxation experiment points to a plastic deformation process. Several mechanisms have been proposed in the literature, such as the relative shear displacement of microfibrils related to the crystalline α-relaxation process [15,20,22,23,32], the motion and/or the annihilation of defects such as kinks, disclinations, dislocations, dispirations and their partial configurations, which allow the transport of a CH_2-group along a chain [4,21,25,33–35], or kink-band formation [32]. It is generally agreed, however, that the creep deformation is not related to a phase transformation or to break-up of crystallites [15,28,29]. An experiment conducted by Grubb et al. [36] supports the idea that inter-microfibrillar slip occurs during creep. After a sample had been loaded for an extended time period at room temperature, it was cooled to 77 K under load and then unloaded. Although the mean position of the Raman peak indicated zero *average* internal stress, the majority of the peak surface moved to a position corresponding to compressive loads. Considering our model (Fig. 3), fraction A will be subjected to compression, since the overstressed tie molecules retract when the sample is unloaded.

The possible influence of chain scission had been investigated by Wang et al. [37]. Using a nitroxide spin trap interdiffused into an SK 60 fibre they determined that during creep at half the breaking stress 0.2 chain scission events per cm of molecular length occurred. This means that only 1 out of 550 molecules was broken in the experiment. The analysis is the same as given by Kausch [4] for the ESR-investigations of polyamide fibres, namely that chain scission is a *consequence* of stress-induced deformation—but not its cause.

The interpretation of our stress relaxation and tensile experiments follows the same lines as developed above. During stress relaxation we observe a decrease in the

number of moderately and highly overstressed chains, whilst the fraction of less highly loaded material increases. The strong loss in the 5–8 GPa range is ascribed to tie-chain pull-out, and the decrease in the number of moderately overstressed chains to *crystal plastic* deformation.

The stress distribution during a tensile test is shown in Fig. 9. The greatest fraction of material is never loaded to more than about 1 GPa. Evidently the number of moderately and highly loaded chain segments increases when the applied stress is increased. It should be noted that beyond an external stress of 1 GPa the combined number of segments stressed at 0.5 and 1 GPa remains relatively constant and accounts for the *low stress peak* found by other researchers [24,29,33].

4.3. Refined molecular model and implications for ultimate strength

The model shown in Fig. 3 is a helpful but rather schematic representation. Taking into consideration all of the above observations and the fact that the different phases are more or less homogeneously distributed over the fibre volume we have constructed a more realistic model (Fig. 10). Despite the high regularity shown by the electron micrograph (Fig. 2), there are also disordered regions and defects which give rise to strain inhomogeneities. The latter are at the origin of the observed large variation of local chain stresses. Their distribution, as it is observed with Raman spectroscopy after 3 h of creep loading at 1.5 GPa, is represented in Fig. 10. The shown section is considered to be representative of the whole fibre.

The disintegration of such a highly oriented structure occurs predominantly through slip along the chain backbones. This is not only reasonable in view of the different strengths of primary and secondary bonds, but is also corroborated by the virtual absence of chain scission events and by the strong rate- and temperature-dependence of the fracture strength σ_b. (This latter increases at room temperature from 1.6 GPa at a strain rate of $7 \times 10^{-6}\,s^{-1}$ to about 3 GPa at $1.8 \times 10^{-2}\,s^{-1}$.) The upper limit to the fibre strength is clearly the strength of (an infinitely long) single chain. If its breaking force is taken as 4 nN [4], a breaking stress of 21 GPa is obtained. A smaller value, $\sigma_b = 7.2$ GPa is cited by Crist [38]. The reason for the difference between theoretical and practical strength is twofold: the presence of the structural irregularities and the large tendency for slip are responsible for the fact that only 6% of the chain segments are loaded up to capacity. In order to increase their number—and thus the fracture stress—the *defects* should be further reduced and the slipping mechanisms on all levels (chain pull-out, crystal plasticity, slip of entire crystalline blocks) made more difficult.

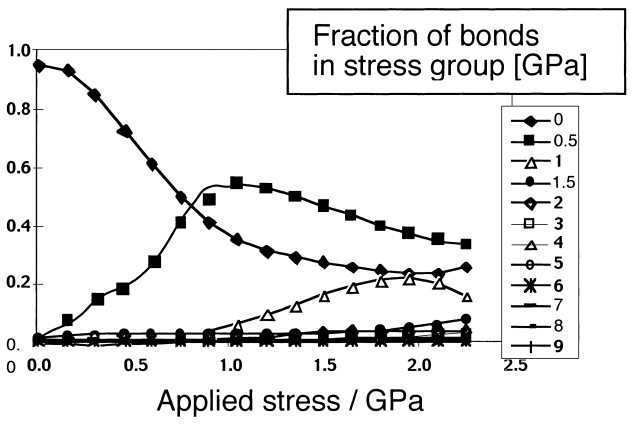

Fig. 9.

Both ways have been followed. The number and influence of defects on strength is reduced by further orienting as-spun UHMWPE fibers at very high temperatures (130–150 °C) resulting in strengths values of 4.6–5.6 GPa [39]. Woods et al. have improved σ_b of UHMWPE by cross-linking through electron irradiation, in particular the fracture strength at low loading rate [40]. As to be expected, the *strain* at break is also reduced by such treatments. Using a different approach, Jacobs [25] achieved a selective cross-linking through interdiffiusion of UV sensitive initiators into the (SK 60) fibre, followed by UV irradiation. The creep rate was notably reduced, unfortunately σ_b and ε_b as well (probably because of *freezing-in* of just those structure inhomogeneities, which give rise to stress concentration upon loading). A selective influence on chain slipping was also obtained by an introduction of methyl branches into the chain backbone. By increasing the methyl branch content from 1 to 12 per 1000 CH_2, Ohta and Yasuda [41] reduced the chain-to-chain slippage but did not affect grain boundary slippage. Tensile strength as well as modulus decreased with increasing the methyl branch content.

5. Conclusions

A structural model consisting of highly extended chains and, mechanically in parallel to these, crystalline regions in series with regions containing correlated defects is found to be most suitable to explain the experimental work done so far on polyethylene fibres. In the SK60 fibre investigated here, a fraction of extended chains of about six percent is loaded to capacity. This fraction increases and the number of defects trapped in the structure decreases as the draw ratio during the production of the fibre is increased. In the beginning of a creep test, the instantaneous elastic modulus of the fibre increases because *defects* are eliminated. Over longer creep times the instantaneous elastic modulus decreases as a consequence of tie-chain pull-out.

The reason for the discrepancy between theoretically feasible and practically achieved strength and modulus values lies in the complex and non-perfect structure. Some chains are exposed to stresses of up to 10 GPa, which is close to their estimated strength. However, chain rupture is

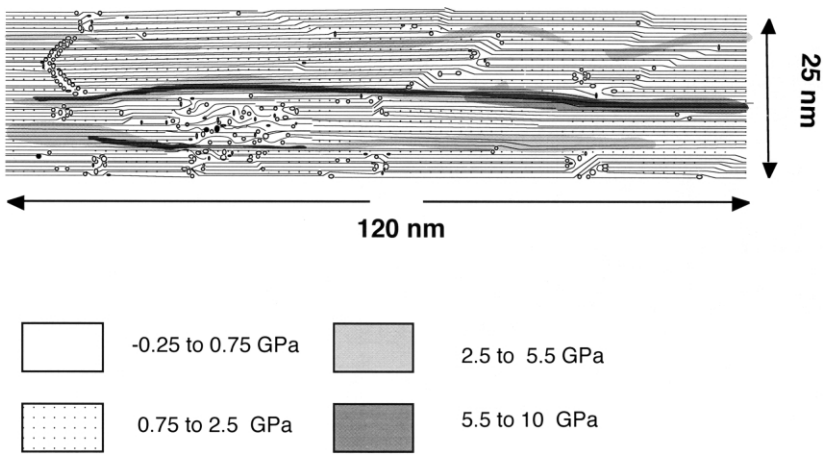

Fig. 10. Refined model of stress distribution in a UHMWE-fibre stressed at 1.5 Gpa.

only considered to be a minor contribution to the deformation mechanisms of the fibres, since only a few chain ruptures can be observed by ESR-spectroscopy. Chain slippage and slippage of complete crystalline areas are of much higher importance. Their effect on the creep properties of the fibres is certainly reduced by the use of line of hybrid materials as for instance tissues woven of UHMWE and Kevlar® fibres. In another line of research the toughness, strength and drapability of highly oriented fibres are put to excellent use in the form of self-reinforced composites or hot compacted fibres [13,14,42]. Despite the basic compatibility between a highly oriented fibre and a matrix of identical chemical composition, a careful balance must be sought between melting and recrystallisation of fibre material in order to ensure optimum stress transmission and maintaining the state of ultra high orientation.

Acknowledgements

The authors wish to thank C. Bastiaansen (ETH Zürich), D. Bassett, L. Boogh (EPFL Lausanne), M.J.N. Jacobs and R.J. Meier (DSM Holland), H. Münstedt (Univ. Erlangen), K. Nakamae (Univ. of Kobe), P. Smith (ETH Zürich) and I.M. Ward for stimulating discussions. DSM High Performance Fibres are thanked for providing the SK60 fibres.

References

[1] Stuart HA, editor. Die Physik der Hochpolymere, Bd. III, Ordnungszustände und Umwandlungserscheinungen in festen hochpolymeren Stoffen. Berlin: Springer; 1955.
[2] Ward IM, Hadley DW. An introduction to mechanical properties of solid polymers. Cichester: Wiley; 1993.
[3] Ward IM, editor. Oriented polymers, vols. 1 and 2. London: Appl. Science Publishers; 19821986.
[4] Kausch HH. Polymer fracture, 2nd ed. Berlin: Springer; 1987.
[5] Ciferri A, Ward IM, editors. Ultra-high modulus polymers. London: Applied Science; 1978.
[6] Hongu T, Phillips GO. New fibers, 2nd ed. Cambridge: Woodhead Publish. Ltd; 1997.
[7] Porter RS, Wang LH. JMS-Rev Macromol Chem Phys 1995;C35:63.
[8] Jiang H, Adams WW, Eby RK. High performance polymer fibers. In: Cahn RW, Haasen P, Kramer EJ. Materials science and technology. New York: VCH, Chapter 13.
[9] Yeh WY, Young RJ. Polymer 1998;40:857.
[10] Capaccio G, Ward IM. Polymer 1974;15:233.
[11] Zwijnenburg A, Pennings AJ. Colloid Polym Sci 1976;254:868.
[12] Smith P, Lemstra PJ, Booij HC. J Polym Sci: Polym Phys Ed 1981;19:877.
[13] Jacobs O, Mentz N, Poeppel A, Schulte K. Wear 2000;244:20.
[14] Jordan ND, Olley RH, Bassett DC, Hine PJ, Ward IM. Polymer 2002;43:3397.
[15] Berger L. Thèse No 1704, EPFL Lausanne; 1997.
[16] Tzou DJ, Schmidt-Rohr K, Spiess HW. Polymer 1994;35:4728.
[17] Cheng J, Fone M, Reddy VN, Schwartz KB, Fisher HP, Wunderlich B. J Polym Sci: Polym Phys Ed 1994;37:2683.
[18] Cook JTE, Klein PG, Ward IM, Brain AA, Farrar DF, Rose J. Polymer 2000;41:8615.
[19] Elyashevich GK, Karpov EA, Kudasheva OV, Rosova E. Mech Time-Depend Mater 1999;3:319.
[20] Gibson AG, Davies GR, Ward IM. Polymer 1978;19:683.
[21] Govaert L. Thesis. TU Eindhoven; 1990.
[22] van der Werff H, Pennings AJ. Colloid Polym Sci 1991;269:747.
[23] Wong WF, Young RJ. J Mater Sci 1994;29:520.
[24] Amornsakchai T, Unwin AP, Ward IM, Batchelder DN. Macromolecules 1997;30:5034.
[25] Jacobs MJN. Thesis. TU Eindhoven; 1999.
[26] Nakamae K, Nishino T, Ohkubo H. J Macromol Sci Part B: Macromol Phys Ed 1991;B30:1.
[27] Kausch HH, Langbein D. J Polym Sci: Polym Phys Ed 1973;11:1201.
[28] Grubb DT, Prasad K. Macromolecules 1992;25:4575–82.
[29] Moonen JAHM, Roovers WAC, Meier RJ, Kip BJ. J Polym Sci: Polym Phys Ed 1992;30:361.
[30] Young RJ. In: Fawcett AH, editor. Polymer spectroscopy. Chichester: Wiley; 1996.
[31] Wilding MA, Ward IM. Polymer 1978;19:969.
[32] Mjasnikova LP, Marikhin VA, Ivan'kova EM, Yakushev PN. J Macromol Sci Part B: Macromol Phys Ed 2001;B38:859.
[33] Boogh L. Thèse No 1091, EPFL Lausanne; 1993.
[34] Reneker DH, Mazur J. Polymer 1988;29:3.
[35] Schuppert AA. Makromol Chem, Theory Simul 1993;2:643.

[36] Grubb DT, Li Z-F. Polymer 1992;33:2587.
[37] Wang D, Klaassen AAK, Janssen GE, de Boer E, Meier RJ. Polymer 1995;36:4193.
[38] Crist B. Annu Rev Mater Sci 1995;25:295.
[39] Marikhin VA, Mjasnikova LP, Zenke D, Hirte P. Polym Bull 1984;12:287.
[40] Woods DW, Busfield WK, Ward IM. Polym Commun 1984;25:298.
[41] Ohta Y, Yasuda H. J Polym Sci Part B: Polym Phys 1994;32:2241.
[42] Hine PJ, Ward IM, Jordan ND, Olley RH, Bassett DC. Polymer 2003;44:1117.